J Mater Sci: Mater Med (2011) 22:1933–1945
DOI 10.1007/s10856-011-4375-7

Analysis of the cytotoxicity of differentially sized titanium dioxide nanoparticles in murine MC3T3-E1 preosteoblasts

Yilin Zhang · Weiqiang Yu · Xinquan Jiang · Kaige Lv · Shengjun Sun · Fuqiang Zhang

Received: 11 March 2011 / Accepted: 6 June 2011 / Published online: 18 June 2011

Abstract There is an increased use of nanophase titanium dioxide (TiO_2) in bone implants and scaffolds. However, nano-debris is generated at the bone-biomaterial interface. Therefore, TiO_2 nanoparticles (NPs) of many sizes were investigated for cytotoxic effects on murine MC3T3-E1 preosteoblasts. These TiO_2 NPs induced a time- and dose-dependent decrease in cell viability. There was a significant increase in lactate dehydrogenase (LDH) release, apoptosis and mitochondrial membrane permeability following short-term exposure of the cells to TiO_2 NPs. These NPs also increased granulocyte-macrophage colony stimulating factor (GM-CSF) and granulocyte colony-stimulating factor (G-CSF) gene expression. Compared with the 32 nm TiO_2 NPs, 5 nm TiO_2 NPs were more toxic, induced more apoptosis, increased mitochondrial membrane permeability and stimulated more GM-CSF expression at a high concentration ($\geq$100 μg/ml). The results implied that the differential toxicity was associated with variations in size, so more attention should be given to the toxicity of small NPs for the design of future materials for implantation.

Y. Zhang · W. Yu · X. Jiang · K. Lv · S. Sun · F. Zhang (✉)
Department of Prosthodontics, Ninth People's Hospital, Shanghai Key Laboratory of Stomatology, Shanghai Jiao Tong University School of Medicine, Shanghai, People's Republic of China
e-mail: fqzhang@vip.163.com

X. Jiang
Oral Bioengineering Lab, Shanghai Research Institute of Stomatology, Ninth People's Hospital, Shanghai Key Laboratory of Stomatology, Shanghai Jiao Tong University School of Medicine, Shanghai 200011, China

1 Introduction

Nanobiomaterials show great potential in the application of bone prostheses, bone engineering scaffolds and bone implants because of the special properties of their nanometric surface topography, such as high specific surface area, roughness and chemical composition [1, 2]. Titanium oxide nanoparticles (TiO_2, NPs) are used in pigments, sunscreens, cosmetics and more recently, in biomaterials [3, 4]. Compared to conventional TiO_2 formulations, a nanophase TiO_2 layer on the surface of implants can modulate protein adsorption, stimulate cell adhesion, enhance alkaline phosphatase activity, promote bone mineralisation at the bone–biomaterial interface and improve osteointegration in vivo [5–7]. Furthermore, ceramics made from TiO_2 NPs can induce bone-like apatite formations, stimulate osteoconductivity and can bond directly to living bone in a shorter period of time after implantation [8–10]. TiO_2 NPs have also been reported as potential fillers in polymeric materials to improve the strength, toughness and wear of bone-engineered scaffolds [11–13].

Bone prostheses and orthopaedic or dental implants containing NPs may release nano-debris at the bone–biomaterial interface into the microenvironment [11]. Possible harmful effects of these NPs on their local environment and the health of the patient are still uncertain. Certain routes of exposure to TiO_2 NP absorption, such as inhalation, have proven to be toxic. TiO_2 NPs exhibit a different toxic potential compared to bulk material or conventional particles [14, 15]. TiO_2 NPs have been shown to have a greater capacity to stimulate interleukin-8 (IL-8) release from lung epithelial cells and cause lung inflammation when compared to fine TiO_2 particles [16, 17]. The increased toxicity may be elicited by the high surface-to-mass ratio of the NPs. Furthermore, it was reported that 20 nm particles

were genotoxic, while 200 nm particles did not induce toxicity [18]. To date, most in vitro studies have focused on the comparison between TiO_2 micron- or submicron-size particles and NPs [18–20]. However, comparisons of TiO_2 NPs of many sizes have been seldom mentioned. Recently, experts have reported that metal oxide particles less than 30 nm in diameter underwent dramatic changes in crystalline structure that enhanced their interfacial reactivity [21]. The surface area of the NPs was also reported to increase noticeably as the particle size decreased to less than 10 nm [22]. These observations suggest that nanotoxicological studies might be better focused on a smaller set of NPs with unique nanoscale properties, which was the focus of the present report.

Studies have shown that debris can induce bone loss, loosen implants and sometimes cause clinical failure of bone prostheses [23–25]. In addition, there is growing evidence that debris can directly affect cells of the osteoblast lineage [26, 27]. Therefore, the adverse effects of NPs on peri-implant cells, especially bone cells, should be determined. Only a few studies have been conducted on the response of osteoblasts to nanophase TiO_2 debris. An early study reported that nanophase TiO_2 particles (23 nm) caused a well-spread cell morphology and increased cell viability within 2 or 6 h [12], while another study concluded that the presence of TiO_2 NPs (15 nm) in the extracellular area surrounding osteoblast cells led to a decrease in cell proliferation after 24 h [28]. These disparities might have been caused by differences in size or the types of TiO_2 NP crystal structures analysed (one study used a combination of rutile and anatase and the other used anatase). Cellular organelle damage and phenotypical changes (e.g., the release of cytokines and proteases) in osteoblast lineages in the presence of TiO_2 NPs have scarcely been studied [11].

Herein, 5 and 32 nm TiO_2 NPs (purity: 99%, anatase; np5 and np32, respectively), which have identical phases, were evaluated for cytotoxic effects on murine preosteoblast MC3T3-E1 cells. Changes in mitochondrial membrane permeability and pro-inflammatory gene expression, such as granulocyte-macrophage colony stimulating factor (GM-CSF), were also investigated to reveal possible mechanisms of toxicity induced by exposure of the cells to TiO_2 NPs.

2 Materials and methods

2.1 Characterisation and preparation of particles

Titanium oxide nanoparticles (TiO_2 NPs; purity: 99% anatase) of 5 and 32 nm in diameter were purchased from Alfa Aesar (Ward Hill, MA, USA). TiO_2 particles were weighed, sterilised by heating to 120°C for 2 h, and added to cell culture medium. NPs in the culture medium were investigated using transmission electron microscopy (TEM) to determine the shape and aggregation. X-ray diffractometry graphs were obtained using an X-ray Diffractometer (Bruker-Axs, Germany) with a copper Kα radiation at 40 kV and 100 mA. The scans were recorded on a KEVEX detector between 20° (2θ) and 80° (2θ) with a 10°/min scan speed. The results of the XRD spectra were compared to TiO_2 standards (anatase and rutile; JCPDS No. 21-1272 and JCPDS No. 21-1276). Prior to the NP addition to the cells, the particles were sonicated for at least 10 min to produce a less-aggregated and uniform suspension in culture medium.

2.2 Cell culture

MC3T3-E1 murine preosteoblasts (subclone 14, obtained from the Chinese Academy Of Science Cell Bank and maintained in our research lab) were cultured in Alpha-Minimum Essential Medium (a-MEM), supplemented with 10% foetal bovine serum and 1% penicillin/streptomycin (PS) in a humidified incubator (37°C and 5% CO_2). The cells were incubated for 24 h prior to exposure to the particles, and the culture medium was changed every 2 or 3 days. Cells free of NPs served as the control group throughout each assay.

2.3 Cell viability and cytotoxicity assays

The tetrazolium salt MTT method and lactate dehydrogenase (LDH) assay were used to determine TiO_2 NP cytotoxicity because trials with more than one assay are recommended to determine cell viability and cytotoxicity [29]. The viability was assessed using the tetrazolium salt MTT method; a total of 4×10^4 cells/ml was plated in 24-well plates. After 24 h, different concentrations of NPs ranging from 0 to 500 μg/ml were added to the wells, and the culture was further incubated for 24, 48, or 72 h. After this treatment, the medium was changed, and the cells were incubated with 0.5 mg/ml MTT (Sigma-Aldrich) under normal culture conditions for 4 h. Subsequently, the medium was removed, and 200 μl DMSO was added to each well. The plates were shaken for 10 min, the solutions were transferred to a 96-multiwell plate, and the absorbance of each solution was measured at 490 nm via a spectrophotometer (BioTek, Elx 800, Winooski, VT, USA). Absorbance values were also corrected with an NP blank. Cell cytotoxicity was assessed by measuring the release of LDH from the cytosol of damaged cells into the medium. In addition, 4×10^4 cells/ml were seeded in a 24-well plate, allowed to attach for 24 h, and treated with different NP concentrations ranging from 0 to 500 μg/ml for 24, 48, or 72 h. LDH release was assayed with the CytoTox 96 non-

radioactive assay (Promega, Madison, WI, USA) according to the manufacturer's instructions.

2.4 Annexin V apoptosis detected by a flow cytometric assay

MC3T3-E1 preosteoblasts were seeded in 6-well plates (4×10^4 cells/ml) and incubated for 24 h. The cells were then treated with different concentrations of TiO_2 NPs ranging from 0 to 500 μg/ml for another 24 h. Cells were trypsinized with 0.125% trypsin solution, washed with PBS and collected by centrifugation (1000 rpm for 5 min). Then cells resuspended in binding buffer and stained with both Annexin V-FITC and propidium iodide (PI) (Annexin V-FITC Apoptosis Detection Kit, BioVision, USA). The cell suspension was ready for the analysis by the flow cytometry (Becton-Dickinson, San Jose, CA, USA). The cells were then analysed for Annexin V using the fluoresceinisothiocyanate (FITC) signal detector (FL1) and PI using the phycoerythrin emission signal detector (FL2).

2.5 TEM analysis

MC3T3-E1 preosteoblasts were cultured at 37°C in 6-well plates as described above. After 24 h, the cells were treated with TiO_2 NPs (10 and 100 μg/ml, moderately cytotoxic doses) for another 24 h and then fixed with glutaraldehyde at 4°C for 1 h. After further fixation with osmium acid, the cells were dehydrated with pyruvic acid and coated with epon. The samples were then examined by TEM.

2.6 Mitochondrial membrane permeability assay

Cells were initially seeded in 6-well plates for 24 h and treated with TiO_2 NPs (from 0 to 100 μg/ml, moderately cytotoxic doses) for another 24 h. Changes in mitochondrial membrane permeability were detected using the Mitochondria Staining Kit (Sigma-Aldrich) according to the manufacturer's instructions. The staining mixture was prepared by mixing the staining solution with an equal volume of α-MEM, and the cells were then incubated in the staining mixture (2 ml/well) for 20 min at 37°C in a humidified atmosphere containing 5% CO_2. Afterwards, the cells were washed with growth medium twice and then observed using an epifluorescence microscope (IX-71, Olympus).

2.7 RNA extraction and real-time quantitative RT-PCR analysis

Following the treatment with NPs for 24 and 48 h, total cellular RNA was extracted using the TRIzol Plus RNA Purification Kit (Invitrogen, USA) according to the recommended protocol. The quantity and quality of the RNA obtained was analysed using a NanoDrop 1000 spectrophotometer (Thermo Scientific, San Jose, CA, USA), according to the manufacturer's instructions. The extracted RNA was subsequently reverse transcribed to cDNA using a PrimeScript_RT reagent kit (Takara Bio, Shiga, Japan). The gene-specific primers for GM-CSF, granulocyte colony-stimulating factor (G-CSF), IL-1, tumour necrosis factor alpha (TNFα) and the calibrator reference gene β-actin were synthesised commercially (Shengong, Co. Ltd., Shanghai, China). The specific primer sets are outlined in Table 1. All quantitative RT-PCR (RT-qPCR) reactions were performed with a MyiQ Single-Colour Real-Time PCR Detection System (Bio-Rad Laboratories, USA). For quantitative PCR, 10 μl SYBR Premix Ex Taq™, 0.4 μl of each forward and reverse primer and 1 μl cDNA template were used in a final reaction volume of 20 μl. Cycling conditions included an initial denaturation step of 180 s at 95°C followed by 40 cycles of 10 s at 95°C, 30 s at 60°C and 30 s at 72°C. Data collection was enabled at 72°C in each cycle, and the C_T (threshold cycle) values were calculated using iQ5 software. Analysis was based on calculating the relative expression level of these genes compared to the expression of the controls at 24 and 48 h ($n = 4$). The level of expression was normalised to β-actin.

Table 1 Nucleotide sequences for real-time RT-PCR primers

Gene	Primer sequence (forward/reverse)	Product size (bp)	Annealing temperature (°C)
IL-1	5′-CAACTGTGAAATGCCACC-3′	176	60
	5′-GTGATACTGCCTGCCTGA-3′		
GM-CSF	5′-GCCATCAAAGAAGCCCTGAA-3′	113	60
	5′-GCGGGTCTGCACACATGTTA-3′		
G-CSF	5′-GGGAAGGAGATGGGTAAAT-3′	147	60
	5′-GGAAGGGAGACCAGATGC-3′		
TNFα	5′-CCTCCTGGCCAACGGCATGG-3′	196	60
	5′-GCAGGGGCTCTTGACGGCAG-3′		

2.8 Statistical analysis

The data were expressed as the mean ± the standard deviation (SD). Data comparisons were performed using a standard analysis of variance (ANOVA) followed by Tukey's or Dunnett's T3 test for multiple comparisons. The independent sample t test was used to compare two-group variables; $P < 0.05$ was considered statistically significant. For cell cytotoxicity experiments, value of $P < 0.01$ was considered significant. Every experiment was repeated at least three times. The statistical analyses were performed using SPSS 11.0 software (SPSS, Chicago, IL, USA).

3 Results

3.1 Particle characterisation

The TEM morphological assessment (Fig. 1a) showed that np32 was larger and had a smaller surface area-to-volume ratio compared to np5. In the presence of the cell culture medium with 10% FBS, both np5 and np32 were found in aggregates. Most np32 particles were round with a smooth surface, while np5 appeared similar to irregularly shaped platelets. The XRD patterns (Fig. 1b) of the two particle samples indicated that they were primarily in the anatase phase with some rutile phase characteristics, and all of their diffraction peaks were assigned according to standard anatase and rutile. There were no significant differences between np5 and np32 with respect to the phase.

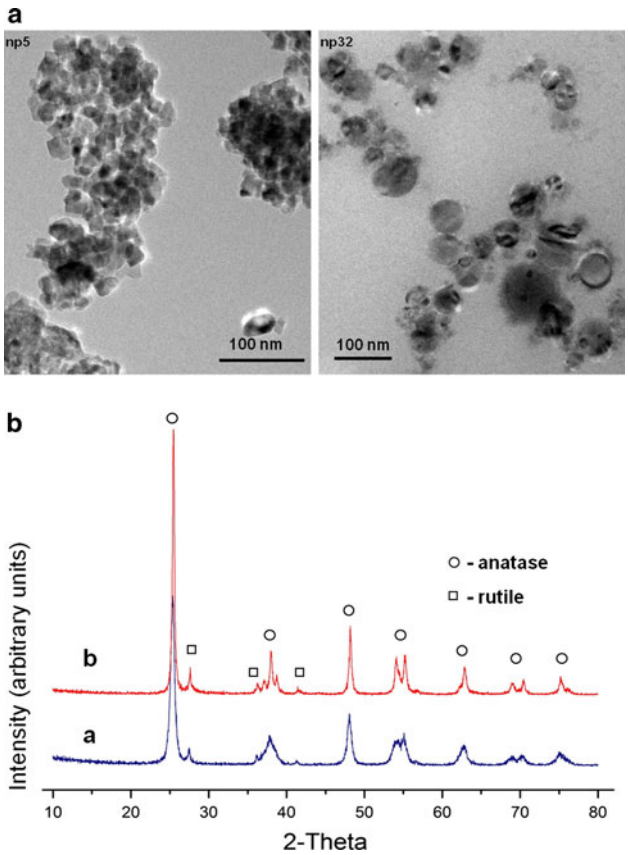

Fig. 1 Characteristics of TiO_2 nanoparticles. **a** TEM images of np5 and np32. **b** XRD patterns of np5 and np32

3.2 Cell cytotoxicity assay

The TiO_2 NP-mediated cytotoxicity of MC3T3-E1 preosteoblasts was assayed using the MTT and CytoTox 96 assays. Figure 2a shows the relationship between the optical density and the different sizes and concentrations of the NPs. Compared to the control, the viability of np32 clearly decreased at 50 μg/ml following 24 h exposure, while the viability of np5 began to decrease at a higher NP concentration (100 μg/ml). The two NPs also showed a reduction in viability at low concentrations at longer exposure time. A significant increase in cytotoxicity was also observed for np32 at 5 μg/ml and np5 at 50 μg/ml. The results of the study also showed a slight increase in viability in cells treated with np5 at 5 μg/ml.

At concentrations of 5–500 μg/ml, the two NP sizes induced a concentration-dependent increase LDH release (Fig. 2b). This assay indicated that the two NP samples caused a significant increase in LDH leakage at a higher concentration (>50 μg/ml) compared to the control. The treatment of cells with particles at 5 μg/ml did not result in significant cell death. Compared to np32, np5 caused greater LDH release at 500 μg/ml in the first 24 h.

3.3 Apoptosis detected by flow cytometry

According to the flow cytometry results, the TiO_2 NPs induced apoptosis (Fig. 3), and the abnormal cells were in the lower right quadrant (Annexin V+ (Ann+)/propidium iodide− (PI−), early apoptosis), upper right (Ann+/PI+, terminal apoptosis) and upper left (Ann−/PI+, necrosis). In the control group, nearly no apoptosis occurred after 24 h cultivation. However, when the cells were treated with TiO_2 NPs, the numbers of apoptotic cells increased as the NP concentration increased. At 500 μg/ml, both np5 and np32 caused significant increases in the numbers of apoptotic cells compared to the control group. The highest rate of apoptotic cells reached 19.84% when cells were treated with 500 μg/ml np5. These results demonstrate that np5 induced greater apoptosis than np32 at 500 μg/ml. It is possible that apoptosis was the mechanism of cell death.

3.4 Observation of internalisation and apoptosis by TEM

TEM microphotographs (Fig. 4) showed that MC3T3-E1 preosteoblasts (4×10^4 cells/ml) treated with 10 or

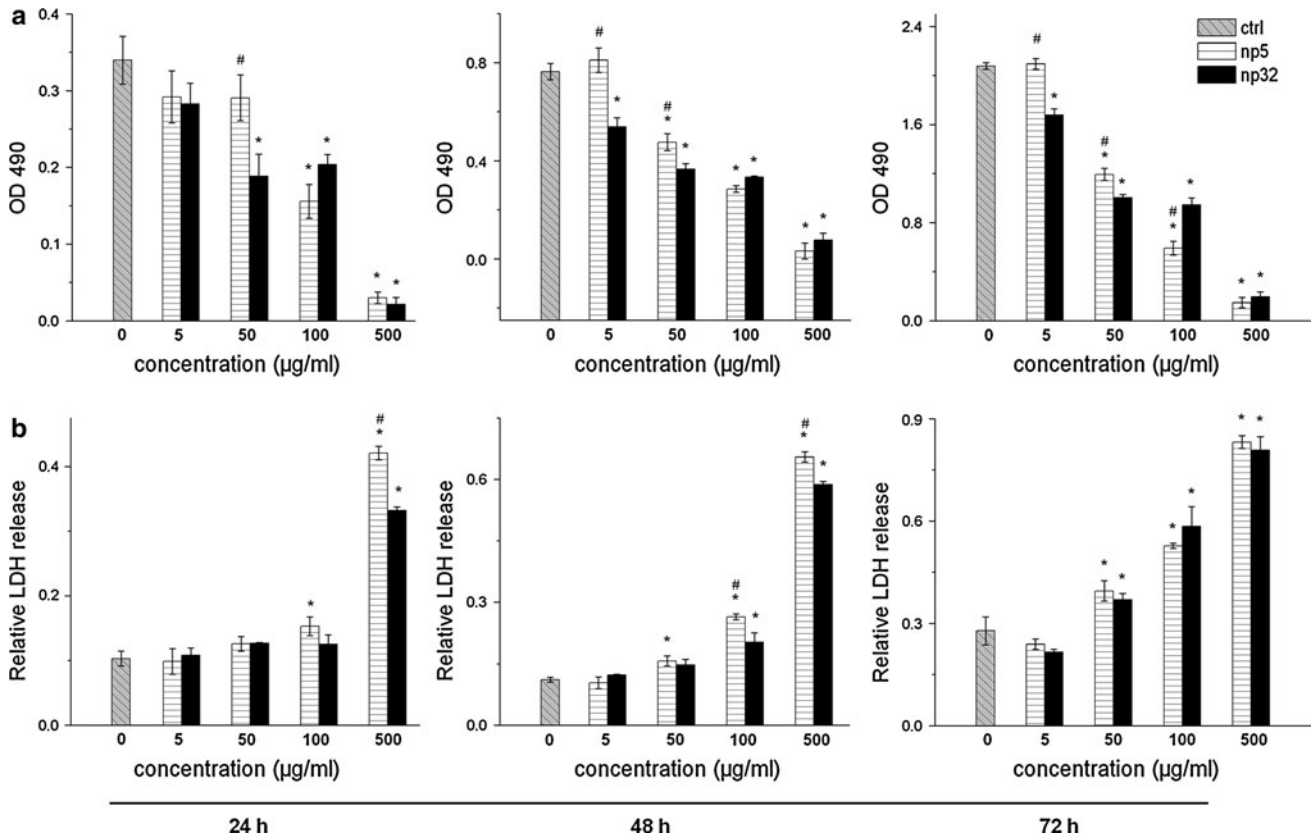

Fig. 2 Effect of np5 and np32 TiO_2 NPs on cell survival based on the MTT (**a**) and CytoTox 96 (**b**) assays. Cells were treated with different nanoparticle concentrations (5–500 μg/ml) for 24, 48, or 72 h, respectively. $n = 3$; *, Significantly different compared to control (no particles); #, significant difference between np5 and np32 in the individual group for each concentration, $P < 0.01$

100 μg/ml TiO_2 NPs formed intracellular vesicles containing endocytosed material in the cytoplasm. There were also visible changes in the cell membrane when endocytosis occurred (Fig. 4a). In all groups, TiO_2 NPs agglomerated on both the surface and inside the cells and vesicles, while irregular-shaped aggregates remained in the cytoplasm but not in the nucleus. Compared to the control, 10 μg/ml TiO_2 NPs (especially np32) did not stimulate visible cellular organelle changes. When the cells were treated with 100 μg/ml np5 or np32 (especially np5) for 24 h, a number of mitochondria swelled, vacuoles appeared and karyoplasms were found concentrated in some samples (Figs. 4d, 5). Therefore, the TEM results indicate that preosteoblast cells function to take up TiO_2 NPs and that apoptosis appears at 100 μg/ml np5 and 100 μg/ml np32 after 24 h.

3.5 Changes of mitochondrial membrane permeability

JC-1 is a potentiometric dye that changes mitochondrial membrane permeability as J-aggregates transition to JC-1 monomers. In healthy cells with a normal mitochondrial membrane potential gradient, JC-1 spontaneously forms red fluorescent J-aggregates, whereas in apoptotic or unhealthy cells, JC-1 remains in the green fluorescent monomeric form. Changes in mitochondrial membrane permeability were evaluated after a 24 h treatment with TiO_2 NPs (Fig. 6). Positive control cells treated with 0.4 μl valinomycin for 30 min had drastically increased mitochondrial membrane permeability. Figure 6 illustrates that the two TiO_2 NPs (especially np5) increased mitochondrial membrane permeability at 100 μg/ml. Compared to the control, cells treated with 10 μg/ml TiO_2 NPs displayed almost no change in mitochondrial membrane permeability.

3.6 Pro-inflammatory response to NPs

To investigate the effect of TiO_2 NPs on the expression of GM-CSF, G-CSF, IL-1 and TNFα in preosteoblasts, real-time RT-qPCR analysis was performed at defined time points (24 or 48 h) using moderately cytotoxic doses of TiO_2 NP (10 and 100 μg/ml). The presence of TiO_2 NPs (especially np5) clearly influenced GM-CSF expression (Fig. 7a); GM-CSF mRNA was dramatically increased in cells exposed to np5 and np32 at 100 μg/ml for 24 h (50.53 and 12.71 fold, respectively) and 48 h (28.83 and 7.32 fold,

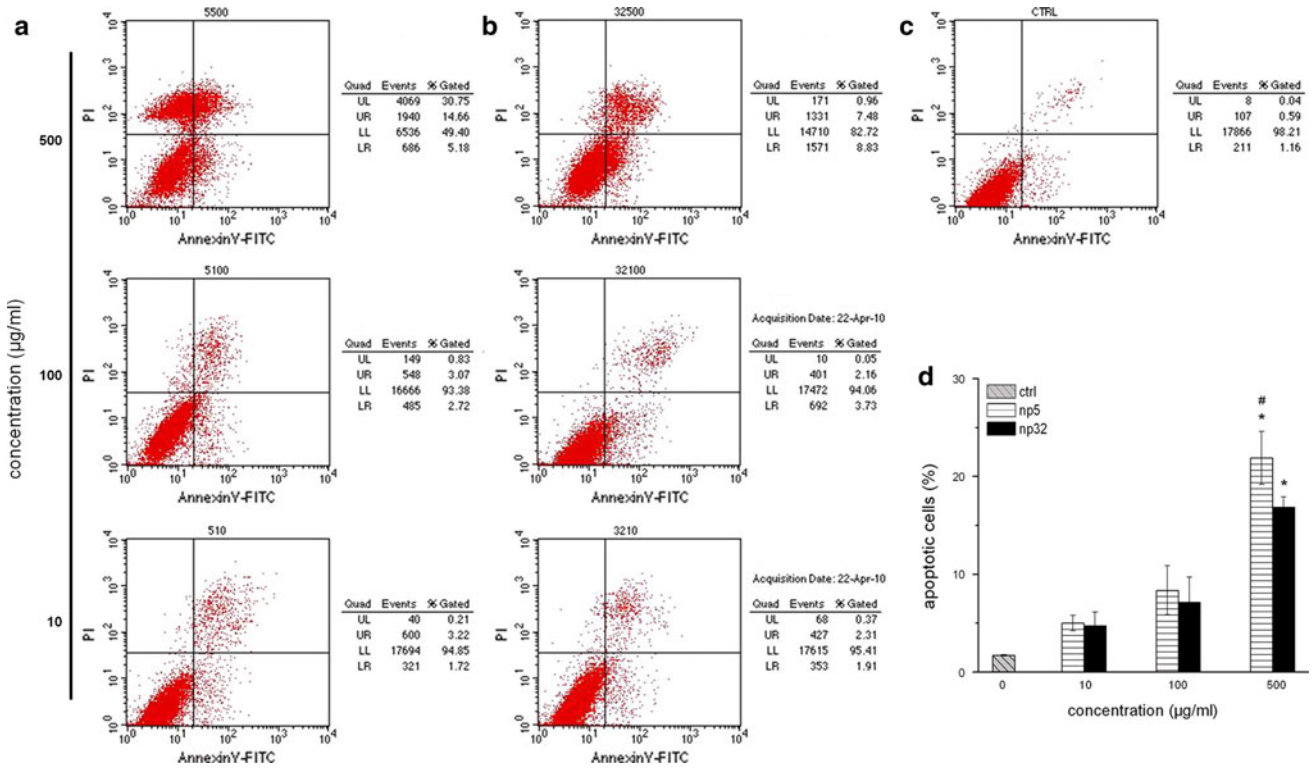

Fig. 3 Flow cytometric analysis of MC3T3-E1 preosteoblast apoptosis induced by TiO_2 nanoparticles for 24 h. **a** np5, **b** np32, **c** control, **d** bar graph to present the number of apoptotic cells ($n = 3$). *, Significantly different compared to control (no particles); #, significant difference between np5 and np32 in the individual group for each concentration, $P < 0.05$

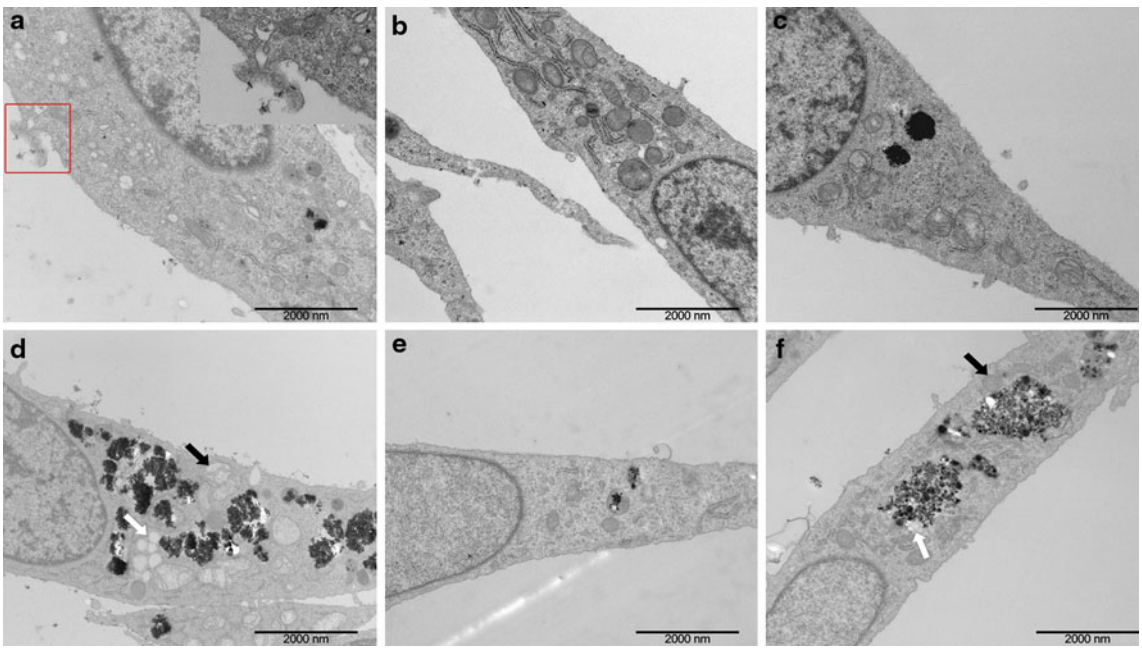

Fig. 4 TEM preparations after 24 h. **a** endocytosis of TiO_2 NPs, **b** control (untreated) cells, **c** and **d** MC3T3-E1 preosteoblasts after treatment with 10 or 100 µg/ml np5, **e** and **f** MC3T3 cells stimulated with 10 or 100 µg/ml np32. TEM of cells treated with TiO_2 NPs **d** and **f** showing swollen mitochondria (*black arrow*) and vacuoles (*white arrow*)

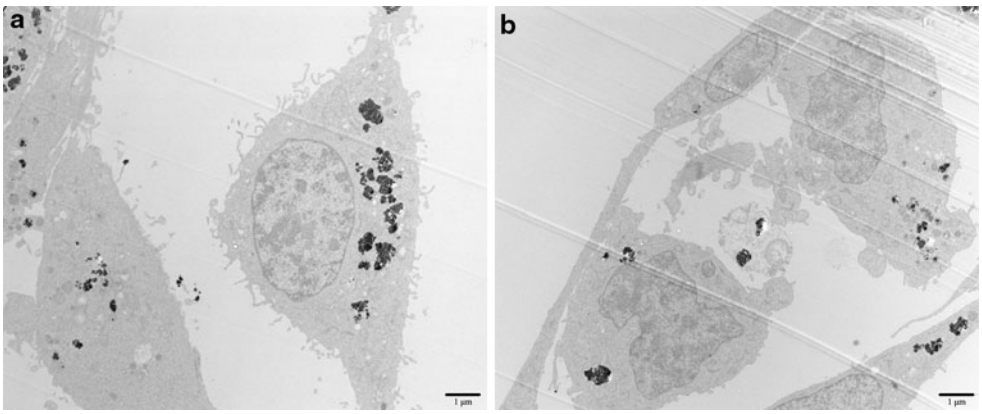

Fig. 5 Apoptosis of MC3T3-E1 preosteoblasts after treatment with 100 μg/ml TiO_2 NPs for 24 h. **a** early apoptosis, **b** terminal apoptosis

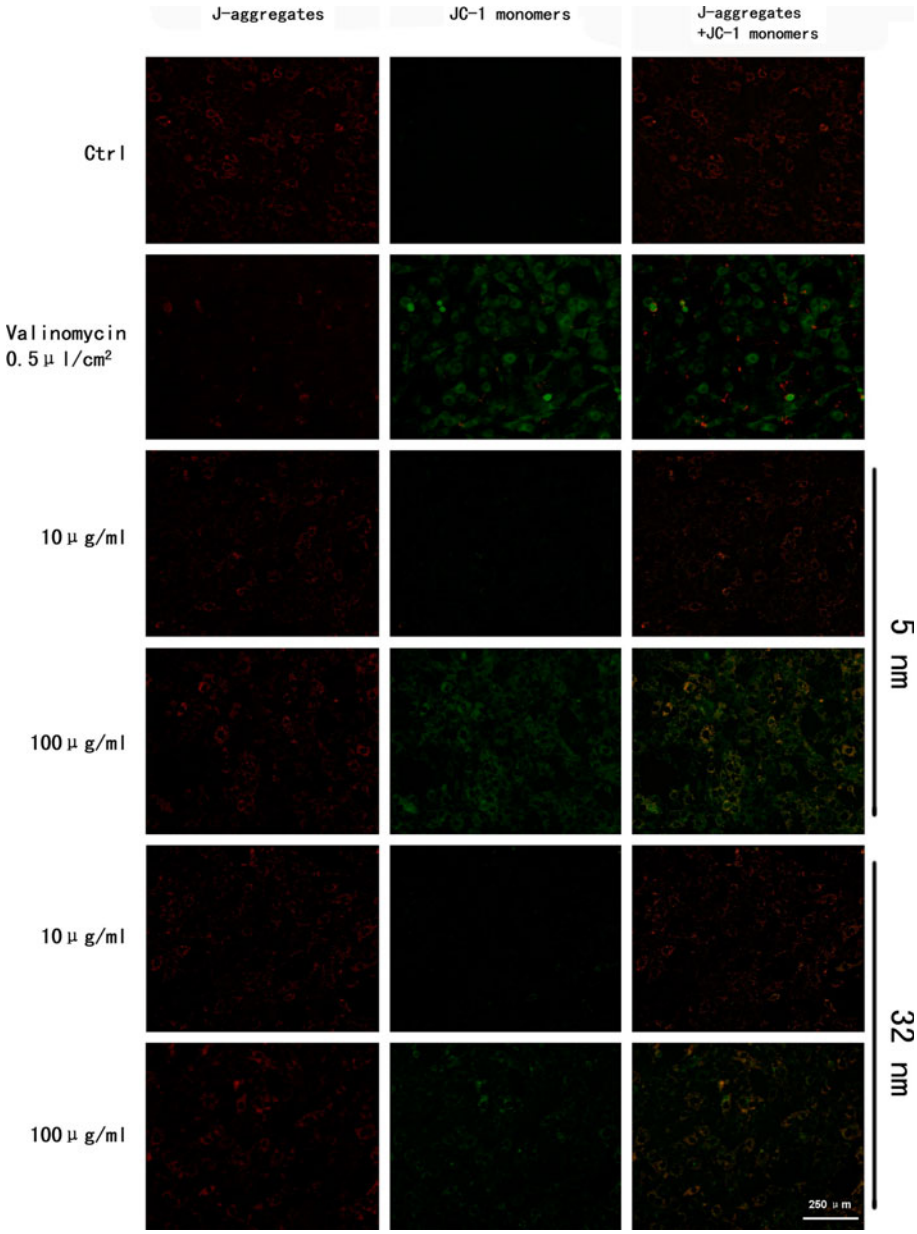

Fig. 6 Effect of TiO_2 nanoparticles on the inner mitochondrial membrane permeability. MC3T3-E1 preosteoblasts were treated with TiO_2 nanoparticles for 24 h

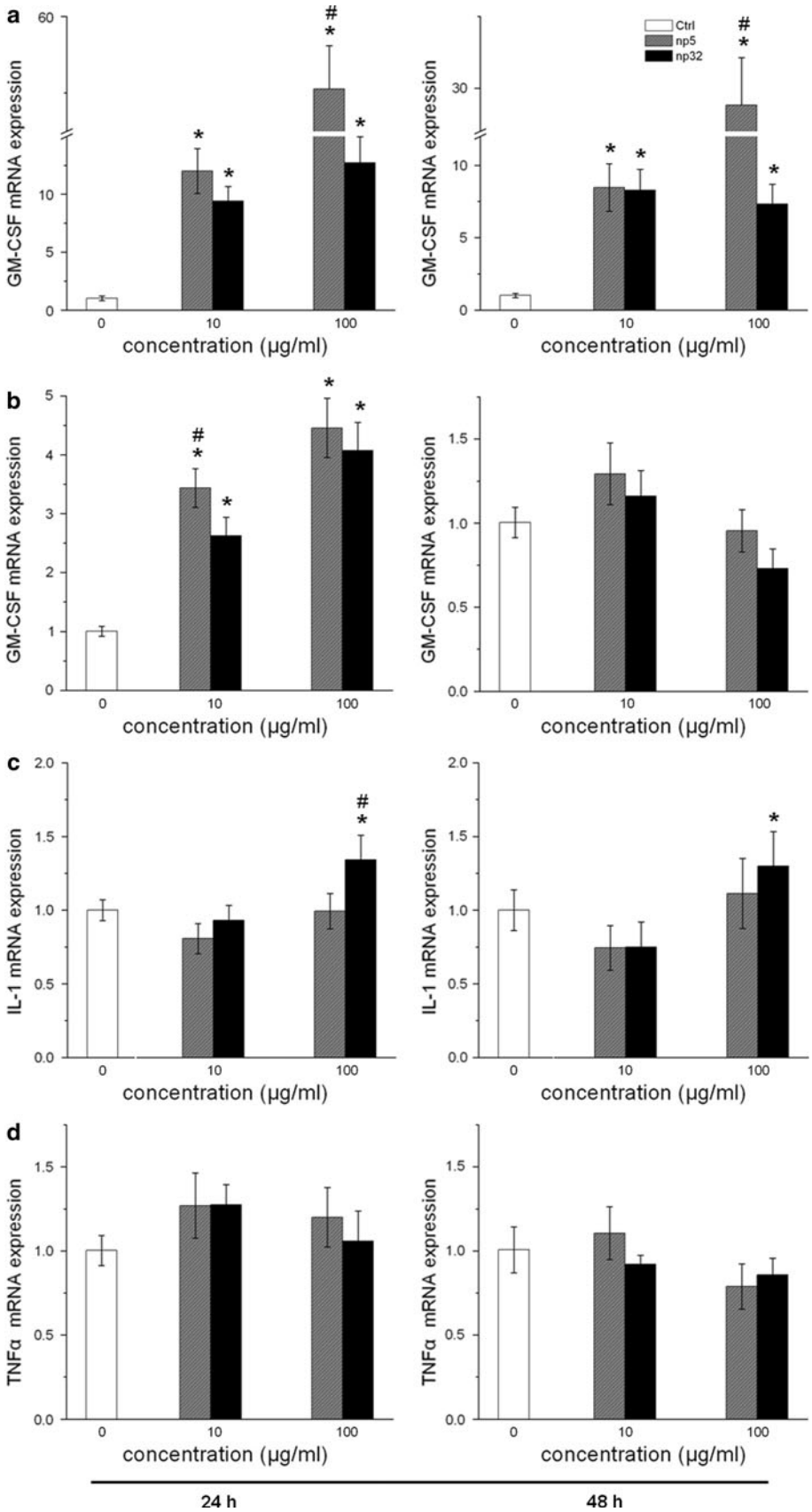

Fig. 7 Evaluation of pro-inflammatory gene expression in MC3T3-E1 preosteoblasts after treatment with TiO_2 NPs for 24 and 48 h: **a** GM-CSF, **b** G-CSF, **c** IL-1 and **d** TNFα. Cells were exposed to np5 or np32 TiO_2 (10 or 100 μg/ml). Data are presented as the mean ± SD ($n = 3$); *, Significantly different compared to control (no particles); #, significant difference between np5 and np32 in the individual group for each concentration, $P < 0.05$

respectively). When cells were exposed to 10 μg/ml TiO_2 NPs at defined time points, the increased GM-CSF expression was also significant for both np5 and np32, although np5 only induced significantly higher GM-CSF expression than np32 at 100 μg/ml. Treatment of MC3T3 cells with np5 or np32 at any tested dose for 24 h increased G-CSF expression (100 μg/ml, 4.46 and 4.07 fold, respectively; 10 μg/ml, 3.44 and 2.63 fold, respectively). G-CSF expression following a 24 h treatment with 10 μg/ml np5 was 1.31 fold higher than that following treatment with 10 μg/ml np32 ($P < 0.05$). At 100 μg/ml, np32 induced 1.35 fold greater IL-1 mRNA expression than np5 ($P < 0.05$), and no change was seen in TNFα mRNA expression after TiO_2 NP exposure compared to the control (Fig. 7c, d).

4 Discussion

Although the development of nanotechnology has led to the increased use of nanobiomaterials, such as TiO_2 nanoparticles (TiO_2 NPs), in bone prostheses and orthopaedic and dental implants, the possible harmful effects of TiO_2 NPs to osteoblast-like cells (especially for NPs of different sizes) are relatively unknown [1, 2, 12, 28]. The present study evaluated the cytotoxic effects of 5 and 32 nm TiO_2 NPs (np5 and np32) on the murine preosteoblast cell line MC3T3-E1. The results from this study demonstrated that np5 caused greater apoptosis, induced significantly more mitochondrial damage and stimulated more pro-inflammatory gene expression than np32, suggesting that this differential toxicity was associated with the size of the TiO_2 NPs.

To determine the state of the particles before cellular exposure, the NP morphology and behaviour in cell culture medium was evaluated by TEM; np5 was significantly smaller than np32. As the NP size decreased (typically to diameters less than 20–30 nm), there was an exponential increase in the number of atoms localised at the surface and crystallographic changes, such as lattice contraction or deformation, rearrangements of the surface atoms, or changes in morphology [21]. In the TEM investigation of the nanoparticles, most np32 particles were round, whereas np5 particles were similar to irregularly shaped platelets. These unique nanoscale features affected the interfacial reactivity. TEM also showed the aggregation of both sizes of TiO_2 NPs in the cell culture medium. The aggregation of the differently sized NPs was in line with reports showing similar behaviour by other NPs [19, 26, 30], although these aggregates can still maintain a large surface area and other characteristics of individual NPs [31, 32].

The MTT assay was based on the conversion of tetrazolium salt by mitochondrial dehydrogenases as marker of cell viability [33]. Only a slight change in viability at low NP concentrations was found, while cell viability decreased drastically at higher concentrations (>50 μg/ml). The results presented here using MC3T3-E1 preosteoblasts supported a number of previous studies, which have demonstrated that NP exposure decreases the viability in both a dose- and time-dependent manner using a variety of cell culture systems [34–37]. Hussain et al. have reported that TiO_2 NPs do not produce a significant reduction in viability at doses between 10 and 50 μg/ml in rat liver cells, but they did observe a significant effect at higher concentrations (100–250 μg/ml) [38]. Additionally, increased cytotoxicity was not observed in human bronchial epithelial cells exposed to approximately 20 μg/ml TiO_2 NPs, while significant cytotoxicity was reported in another study using lower concentrations [39, 40]. These differences in results may be because of differences in susceptibility to NPs from one cell line to another. One study using osteoblast cells reported that TiO_2 NPs led to a decrease in cell proliferation, even when an increase in optical density was observed at 25, 50 and 100 μg/ml in UMR106 cells, which were measured using MTT assays [28]. MTT assay could show cytotoxicity after exposure to low NPs concentration of 50 or 5 μg/ml. This phenomenon may be related to mitochondrial damage [41]. Figure 6 clearly showed that particles were potent to cause mitochondrial damage. The present study also displayed a higher absorbance in cells treated with np5 than np32 at lower concentrations (5 and 50 μg/ml) which may be correlated with the cell endocytosis. Liu et al. [42] reported that MTT was not permeable to lipid membranes and was taken into cells through endocytosis. All these factors which may affect the endocytosis of MTT could lead to the cellular MTT reduction. The present study displayed that cells exposed to np5 endocytosed more particles than cells exposed to np32 under identical concentrations. So we believe that cell exposed to np5 may also have endocytosed more MTT than np32 group which may have led to a higher absorbance in cells treated with np5 at lower concentrations. Besides, cell endocytosis requires the energy which may up-regulate the activity of the mitochondrial respiratory chain and finally increase the absorbance value in MTT assay [28, 43, 44]. These assumptions was also supported by a research by Di Virgilio et al. [28]. The author found that TiO_2 NPs would lead to a decrease in osteoblast proliferation even when the increase in absorbance value was observed for MTT and neutral red (RN) assays. During the first 24 h, the two NP samples only caused a marked increase in LDH leakage at 500 μg/ml. With increased exposure time, the two NPs caused an increase in LDH release at a lower concentration (>50 μg/ml) compared to the control. These results indicated that the toxicity increased with increasing amounts of TiO_2 NPs presented to the MC3T3-E1 preosteoblasts.

The MTT and LDH release assays consistently demonstrated that the NP-induced cytotoxic effect was concentration and time dependent and was pronounced at concentrations greater than 50 μg/ml. For the MTT assay, only at higher concentrations (>50 μg/ml) that np5 was more toxic than np32. The LDH assay clearly showed that the NP-induced cytotoxic effect was size dependent, and np5 was more toxic.

Based on previous cytotoxicity tests, 10, 100 and 500 μg/ml TiO_2 NPs were chosen for further study. To quantify apoptotic cells, Annexin V-FITC and PI were used to analyse the number of apoptotic MC3T3-E1 preosteoblasts induced by NPs. During early exposure, np5 induced more apoptosis than np32 at 500 μg/ml, but there was no significant increase in apoptosis with increasing amounts of NPs presented to cells (from 10 to 100 μg/ml). This result was in agreement with the results from the LDH assay. Previous work has demonstrated that the microtubule cytoskeleton is reformed during apoptosis and plays an important role in plasma membrane integrity. After mitochondrial depolarisation, apoptotic microtubule network disorganisation has been associated with increased LDH release as a result of increased plasma membrane permeability [45]. Another study has reported on the concentration-dependent apoptosis of rat peritoneal macrophages treated with hydroxyapatite NPs [46]. Their data suggested that apoptosis could be a mechanism of cytotoxicity for some NPs, such as TiO_2 NPs.

TEM observations demonstrated cellular vesicle formation after treatment with both TiO_2 NP sizes for a 24 h period. Nearly all metal oxide NPs can be endocytosed by cells [28, 34]. Endocytosis occurs through different mechanisms, including phagocytosis, pinocytosis and receptor-mediated endocytosis. The formation of a coated vesicle, clearly visible by TEM, indicated that the uptake of TiO_2 NPs occurred via receptor-mediated endocytosis [47, 48]. It has been speculated that serum proteins are adsorbed onto NP surfaces, facilitating NP binding to the corresponding cell membrane receptors, followed by subsequent cellular uptake [49]. Although NPs were found in aggregates in the cell culture medium, the surface area and size of the NPs seemed to be an important aspect for internalisation [50]. Cell death may occur by either apoptosis or necrosis. Apoptotic cells are generally characterised by a number of morphologic, molecular and biochemical features [51, 52]. The characteristic ultrastructural changes include cytoplasmic crimpling, concentrated karyoplasms and karyon lysis [53, 54]. In this study, TEM images showed that most cells exhibited mitochondrial swelling following treatment with either 100 μg/ml np5 or np32 over 24 h, while some cells showed typical morphological features of apoptosis. Furthermore, 500 μg/ml TiO_2 NPs induced karyotheca breakup (image not show).

Any change in mitochondrial membrane permeability is known to be an early event in apoptosis. After the formation of a permeability transition pore in the mitochondrial membrane, many pro-apoptotic proteins are released from the mitochondria into the cytosol [55]. A mitochondrial staining kit was used to indicate changes in mitochondrial membrane permeability and identify mitochondrial involvement in TiO_2 NP-induced cytotoxicity. Mitochondria are targets for endocytosed particles, and mitochondrial damage can lead to mitochondrial depolarisation and apoptosis. TiO_2 NPs increased mitochondrial membrane permeability in MC3T3-E1 preosteoblasts, as reported in this study. TiO_2 NPs have been suggested to impact mitochondria by forming reactive oxygen species (ROS) in several cell types, such as brain microglia, bronchial epithelial cells and peripheral lymphocytes [37, 56]. ROS can be formed via transition metals, radicals or other chemicals on the particle surface, or as a consequence of the interaction between particles and cellular components [14]. It has been postulated that the NP surface area (even when in the form of aggregates) plays an important role in ROS production. One study has reported a linear correlation between the NP surface area and oxidative stress [57]. This data implied that the different cytotoxicities between np5 and np32 are related to the surface area, and this work also suggested that particle size was a determining factor in NP cytotoxicity.

NPs were also investigated for the ability to stimulate pro-inflammatory gene expression when murine preosteoblasts were exposed to TiO_2 NPs. In many in vivo and in vitro studies, the exposure of cells to particles induced inflammatory effects and stimulated pro-inflammatory gene expression [57–60]. There have been recent discussions about the correlation between nanoparticle size and the pro-inflammatory response. Results from this study indicated that TiO_2 NPs clearly induced the expression of GM-CSF; the GM-CSF mRNA expression level induced by 100 μg/ml np5 was significantly higher compared to the 100 μg/ml np32 sample. Other in vivo studies have also reported higher GM-CSF mRNA expression in response to ultrafine particles compared to larger sized particles [57, 61, 62]. TiO_2 NPs (15 nm) exhibited a greater potential to cause GM-CSF release compared to 50 nm TiO_2 NPs in the epithelial cell line [57]. All of these studies have indicated a strong correlation between particle size and in vitro GM-CSF mRNA expression caused by TiO_2 NPs. TiO_2 NPs have been shown to generate ROS to a greater extent than larger particles, which lead to the increased transcription of pro-inflammatory mediators via intracellular signalling pathways, including calcium disturbances and oxidative stress [39]. Specifically, when particle size decreased to 5 nm, GM-CSF mRNA expression markedly increased, as the NP surface area was noticeably increased. In addition, the internalised NP concentration should be considered in the TiO_2

NP-induced dose-dependent pro-inflammatory response [57]. As studied in this study, higher concentrations of TiO_2 NPs can trigger cells to express higher levels of G-CSF compared to controls. The IL-1 mRNA expression was significant up-regulated in presence of np32 TiO_2 after 24 and 48 h. However, the increase was minimal, it was less than 1.5 fold compared to the non-treated cells. There was no effect on TNFα mRNA expression. This result was consistent with the research of Valles et al. [63]. They reported that TNFα and IL-1 were not detected in the media from osteoblasts exposed to TiO_2 particles for 24 h. But there are some experiments indicated that TiO_2 particles leaded to high expression of TNFα or IL-1 in macrophage and epithelial cell [37, 63, 64]. This disparity in TNFα or IL-1 expression might be caused by differences in cell types.

As a final note, TiO_2 NPs may also affect osteoblast differentiation, matrix formation, or osteoclast recruitment and possibly result in decreased bone formation. These effects were not measured in this work, and further studies will be performed to investigate these effects in MC3T3-E1 preosteoblasts.

5 Conclusions

Results from this study show that TiO_2 NPs (purity: 99%, anatase) induce cytotoxicity in a time- and dose-dependent manner. There was a significant increase in LDH release and apoptosis following early exposure of the cells to high doses of TiO_2 NPs (500 μg/ml). Pro-inflammatory GM-CSF and G-CSF gene expression also increased in response to exposure to TiO_2 NPs. Furthermore, np5 stimulated significantly greater LDH release, mitochondrial damage and apoptosis when compared to np32, which implies that the differential toxicity is associated with the TiO_2 NPs size. Consequently, the effects of TiO_2 NPs on osteoblast cell lines is dependent on the particle concentration and size as well as exposure time. The toxicity of NPs of diameters less than 30 nm should be addressed in the creation of future materials for implantation.

Acknowledgments This work was supported by grants from the Shanghai Leading Academic Discipline Project (No. S30206, T0202) and the Science and Technology Committee of Shanghai (No. 08DZ2271100). The authors would like to thank Xiuli Zhang and Dongxia Ye (Oral Bioengineering Lab, Ninth People's Hospital, Shanghai Jiao Tong University School of Medicine) for their helpful assistance with the experiments.

References

1. Engel E, Michiardi A, Navarro M, Lacroix D, Planell JA. Nanotechnology in regenerative medicine: the materials side. Trends Biotechnol. 2008;26(1):39–47.
2. Streicher RM, Scbmidt M, Fiorito S. Nanosurfaces and nanostructures for artificial orthopedic implants. Nanomedicine. 2007;2(6):861–74. doi:10.2217/17435889.2.6.861.
3. Zhang F, Zheng ZH, Chen Y, Liu XG, Chen AQ, Jiang ZB. In vivo investigation of blood compatibility of titanium oxide films. J Biomed Mater Res. 1998;42(1):128–33.
4. Thrall L. Are red blood cells defenseless against smaller nanoparticles? Environ Sci Technol. 2006;40(14):4327–8.
5. Park J, Bauer S, von der Mark K, Schmuki P. Nanosize and vitality: TiO_2 nanotube diameter directs cell fate. Nano Lett. 2007;7(6):1686–91. doi:10.1021/nl070678d.
6. Popat KC, Leoni L, Grimes CA, Desai TA. Influence of engineered titania nanotubular surfaces on bone cells. Biomaterials. 2007;28(21):3188–97. doi:10.1016/j.biomaterials.2007.03.020.
7. Yu WQ, Jiang XQ, Zhang FQ, Xu L. The effect of anatase TiO_2 nanotube layers on MC3T3-E1 preosteoblast adhesion, proliferation, and differentiation. J Biomed Mater Res A. 2010;94(4):1012–22. doi:10.1002/jbm.a.32687.
8. Kasuga T, Kondo H, Nogami M. Apatite formation on TiO_2 in simulated body fluid. J Cryst Growth. 2002;235(1–4):235–40.
9. Wang XX, Hayakawa S, Tsuru K, Osaka A. Bioactive titania gel layers formed by chemical treatment of Ti substrate with a H_2O_2/HCl solution. Biomaterials. 2002;23(5):1353–7.
10. Wu JM, Hayakawa S, Tsuru K, Osaka A. Low-temperature preparation of anatase and rutile layers on titanium substrates and their ability to induce in vitro apatite deposition. J Am Ceram Soc. 2004;87(9):1635–42.
11. Gerhardt LC, Jell GMR, Boccaccini AR. Titanium dioxide (TiO_2) nanoparticles filled poly(D,L lactid acid) (PDLLA) matrix composites for bone tissue engineering. J Mater Sci Mater Med. 2007;18(7):1287–98. doi:10.1007/s10856-006-0062-5.
12. Gutwein LG, Webster TJ. Increased viable osteoblast density in the presence of nanophase compared to conventional alumina and titania particles. Biomaterials. 2004;25(18):4175–83. doi:10.1016/j.biomaterials.2003.10.090.
13. Hashimoto M, Takadama H, Mizuno M, Kokubo T. Mechanical properties and apatite forming ability of TiO_2 nanoparticles/high density polyethylene composite: effect of filler content. J Mater Sci Mater Med. 2007;18(4):661–8. doi:10.1007/s10856-007-2317-1.
14. Nel A, Xia T, Madler L, Li N. Toxic potential of materials at the nanolevel. Science. 2006;311(5761):622–7. doi:10.1126/science.1114397.
15. Motskin M, Wright DM, Muller K, Kyle N, Gard TG, Porter AE, et al. Hydroxyapatite nano and microparticles: correlation of particle properties with cytotoxicity and biostability. Biomaterials. 2009;30(19):3307–17. doi:10.1016/j.biomaterials.2009.02.044.
16. Monteiller C, Tran L, MacNee W, Faux S, Jones A, Miller B, et al. The pro-inflammatory effects of low-toxicity low-solubility particles, nanoparticles and fine particles, on epithelial cells in vitro: the role of surface area. Occup Environ Med. 2007;64(9):609–15. doi:10.1136/oem.2005.024802.
17. Bermudez E, Mangum JB, Wong BA, Asgharian B, Hext PM, Warheit DB, et al. Pulmonary responses of mice, rats, and hamsters to subchronic inhalation of ultrafine titanium dioxide particles. Toxicol Sci. 2004;77(2):347–57. doi:10.1093/toxsci/kfh019.
18. Singh N, Manshian B, Jenkins GJS, Griffiths SM, Williams PM, Maffeis TGG, et al. NanoGenotoxicology: the DNA damaging potential of engineered nanomaterials. Biomaterials. 2009;30(23–24):3891–914. doi:10.1016/j.biomaterials.2009.04.009.
19. Karlsson HL, Gustafsson J, Cronholm P, Moller L. Size-dependent toxicity of metal oxide particles-A comparison between nano- and micrometer size. Toxicol Lett. 2009;188(2):112–8. doi:10.1016/j.toxlet.2009.03.014.

20. Park S, Lee YK, Jung M, Kim KH, Chung N, Ahn EK, et al. Cellular toxicity of various inhalable metal nanoparticles on human alveolar epithelial cells. Inhal Toxicol. 2007;19:59–65. doi:10.1080/08958370701493282.
21. Auffan M, Rose J, Bottero JY, Lowry GV, Jolivet JP, Wiesner MR. Towards a definition of inorganic nanoparticles from an environmental, health and safety perspective. Nat Nanotechnol. 2009;4(10):634–41. doi:10.1038/nnano.2009.242.
22. Liang GY, Pu YP, Yin LH, Liu R, Ye B, Su YY, et al. Influence of different sizes of titanium dioxide nanoparticles on hepatic and renal functions in rats with correlation to oxidative stress. J Toxicol Environ Health A. 2009;72(11–12):740–5. doi:10.1080/15287390902841516.
23. Oparaugo PC, Clarke IC, Malchau H, Herberts P. Correlation of wear debris-induced osteolysis and revision with volumetric wear-rates of polyethylene—a survey of 8 reports in the literature. Acta Orthop Scand. 2001;72(1):22–8.
24. Urban RM, Jacobs JJ, Tomlinson MJ, Gavrilovic J, Black J, Peoc'h M. Dissemination of wear particles to the liver, spleen, and abdominal lymph nodes of patients with hip or knee replacement. J Bone Joint Surg Am. 2000;82A(4):457–77.
25. Hashiguchi T, Hirano T, Shindo H, Baba K. Wear of alumina ceramics prosthesis. Arch Orthop Trauma Surg. 1999;119(1–2):30–4.
26. Wang JX, Fan YB, Gao Y, Hu QH, Wang TC. TiO_2 nanoparticles translocation and potential toxicological effect in rats after intraarticular injection. Biomaterials. 2009;30(27):4590–600. doi:10.1016/j.biomaterials.2009.05.008.
27. Atkins GJ, Welldon KJ, Holding CA, Haynes DR, Howie DW, Findlay DM. The induction of a catabolic phenotype in human primary osteoblasts and osteocytes by polyethylene particles. Biomaterials. 2009;30(22):3672–81. doi:10.1016/j.biomaterials.2009.03.035.
28. Di Virgilio AL, Reigosa M, de Mele MFL. Response of UMR 106 cells exposed to titanium oxide and aluminum oxide nanoparticles. J Biomed Mater Res A. 2010;92A(1):80–6. doi:10.1002/jbm.a.32339.
29. Fotakis G, Timbrell JA. In vitro cytotoxicity assays: comparison of LDH, neutral red, MTT and protein assay in hepatoma cell lines following exposure to cadmium chloride. Toxicol Lett. 2006;160(2):171–7. doi:10.1016/j.toxlet.2005.07.001.
30. Singh S, Shi TM, Duffin R, Albrecht C, van Berlo D, Hoehr D, et al. Endocytosis, oxidative stress and IL-8 expression in human lung epithelial cells upon treatment with fine and ultrafine TiO_2: role of the specific surface area and of surface methylation of the particles. Toxicol Appl Pharmacol. 2007;222(2):141–51. doi:10.1016/j.taap.2007.05.001.
31. Phenrat T, Saleh N, Sirk K, Tilton RD, Lowry GV. Aggregation and sedimentation of aqueous nanoscale zerovalent iron dispersions. Environ Sci Technol. 2007;41:284–90. doi:10.1021/es061434 9a.
32. Long TC, Tajuba J, Sama P, Saleh N, Swartz C, Parker J, et al. Nanosize titanium dioxide stimulates reactive oxygen species in brain microglia and damages neurons in vitro. Environ Health Perspect. 2007;115:1631–7. doi:10.1289/ehp.10216.
33. Slater TF, Sawyer B, Strauli U. Studies on succinate-tetrazolium reductase systems. 3. Points of coupling of 4 different tetrazolium salts. Biochim Biophys Acta. 1963;77(3):383–93.
34. Di Virgilio AL, Reigosa M, Arnal PM, de Mele MFL. Comparative study of the cytotoxic and genotoxic effects of titanium oxide and aluminium oxide nanoparticles in Chinese hamster ovary (CHO-K1) cells. J Hazard Mater. 2009;177(1–3):711–8. doi:10.1016/j.jhazmat.2009.12.089.
35. Thevenot P, Cho J, Wavhal D, Timmons RB, Tang LP. Surface chemistry influences cancer killing effect of TiO_2 nanoparticles. Nanomedicine. 2008;4(3):226–36. doi:10.1016/j.nano.2008.04.001.
36. Jin CY, Zhu BS, Wang XF, Lu QH. Cytotoxicity of titanium dioxide nanoparticles in mouse fibroblast cells. Chem Res Toxicol. 2008;21(9):1871–7. doi:10.1021/tx800179f.
37. Park EJ, Yi J, Chung YH, Ryu DY, Choi J, Park K. Oxidative stress and apoptosis induced by titanium dioxide nanoparticles in cultured BEAS-2B cells. Toxicol Lett. 2008;180(3):222–9. doi:10.1016/j.toxlet.2008.06.869.
38. Hussain SM, Hess KL, Gearhart JM, Geiss KT, Schlager JJ. In vitro toxicity of nanoparticles in BRL 3A rat liver cells. Toxicol In Vitro. 2005;19(7):975–83. doi:10.1016/j.tiv.2005.06.034.
39. Bhattacharya K, Davoren M, Boertz J, Schins RPF, Hoffmann E, Dopp E. Titanium dioxide nanoparticles induce oxidative stress and DNA-adduct formation but not DNA-breakage in human lung cells. Parti Fibre Toxicol. 2009;6:17. doi:10.1186/1743-8977-6-17.
40. Jeng HA, Swanson J. Toxicity of metal oxide nanoparticles in mammalian cells. J Environ Sci Health A Tox Hazard Subst Environ Eng. 2006;41(12):2699–711. doi:10.1080/10934520600966177.
41. Mosmann T. Rapid colorimetric assay for cellular growth and survival: application to proliferation and cytotoxicity assays. J Immunol Methods. 1983;65(1–2):55–63.
42. Liu Y, Peterson DA, Kimura H, Schubert D. Mechanism of cellular 3-(4,5-dimethylthiazol-2-yl)-2,5-diphenyltetrazolium bromide (MTT) reduction. J Neurochem. 1997;69(2):581–93.
43. Xin X, Zeng T, Dou DD, Zhao S, Du JY, Pei JJ et al. Changes of mitochondrial ultrastructures and function in central nervous tissue of hens treated with tri-ortho-cresyl phosphate (TOCP). Hum Exp Toxicol. 2010. doi:10.1177/0960327110386815.
44. Masoud A, Kiran R, Sandhir R. Impaired mitochondrial functions in organophosphate induced delayed neuropathy in rats. Cell Mol Neurobiol. 2009;29(8):1245–55. doi:10.1007/s10571-009-9420-4.
45. Oropesa M, de la Mata M, Maraver JG, Cordero MD, Cotan D, Rodriguez-Hernandez A et al. Apoptotic microtubule network organization and maintenance depend on high cellular ATP levels and energized mitochondria. Apoptosis. 2011. doi:10.1007/s10495-011-0577-1.
46. Sun J, Ding TT. p53 Reaction to apoptosis induced by hydroxyapatite nanoparticles in rat macrophages. J Biomed Mater Res A. 2009;88A(3):673–9. doi:10.1002/jbm.a.31892.
47. Chithrani BD, Chan WCW. Elucidating the mechanism of cellular uptake and removal of protein-coated gold nanoparticles of different sizes and shapes. Nano Lett. 2007;7(6):1542–50. doi:10.1021/nl070363y.
48. Huajian G, Wendong S, Freund LB. Mechanics of receptor-mediated endocytosis. Proc Natl Acad Sci USA. 2005;102(27):9469–74. doi:10.1073/pnas.0503879102.
49. Chithrani BD, Ghazani AA, Chan WCW. Determining the size and shape dependence of gold nanoparticle uptake into mammalian cells. Nano Lett. 2006;6(4):662–8. doi:10.1021/nl052396o.
50. Limbach LK, Li YC, Grass RN, Brunner TJ, Hintermann MA, Muller M, et al. Oxide nanoparticle uptake in human lung fibroblasts: effects of particle size, agglomeration, and diffusion at low concentrations. Environ Sci Technol. 2005;39(23):9370–6. doi:10.1021/es051043o.
51. Darzynkiewicz Z, Bruno S, Delbino G, Gorczyca W, Hotz MA, Lassota P, et al. Features of apoptotic cells measured by flow-cytometry. Cytometry. 1992;13(8):795–808.
52. Kerr JFR, Wyllie AH, Currie AR. Apoptosis—basic biological phenomenon with wide-ranging implications in tissue kinetics. Br J Cancer. 1972;26(4):239–57.
53. Cheng YY, Huang L, Kumta SM, Lee KM, Lai FM, Tam JSK. Cytochemical and ultrastructural changes in the osteoclast-like giant cells of giant cell tumor of bone following bisphosphonate

administration. Ultrastruct Pathol. 2003;27(6):385–91. doi:10.1080/01913120390248629.
54. Rahman Q, Lohani M, Dopp E, Pemsel H, Jonas L, Weiss DG, et al. Evidence that ultrafine titanium dioxide induces micronuclei and apoptosis in Syrian hamster embryo fibroblasts. Environ Health Perspect. 2002;110(8):797–800.
55. Zhao JS, Bowman L, Zhang XD, Vallyathan V, Young SH, Castranova V, et al. Titanium dioxide (TiO_2) nanoparticles induce JB6 cell apoptosis through activation of the caspase-8/bid and mitochondrial pathways. J Toxicol Environ Health A. 2009;72(19):1141–9. doi:10.1080/15287390903091764.
56. Kang SJ, Kim BM, Lee YJ, Chung HW. Titanium dioxide nanoparticles trigger p53-mediated damage response in peripheral blood lymphocytes. Environ Mol Mutagen. 2008;49(5):399–405.
57. Hussain S, Boland S, Baeza-Squiban A, Hamel R, Thomassen LCJ, Martens JA, et al. Oxidative stress and proinflammatory effects of carbon black and titanium dioxide nanoparticles: role of particle surface area and internalized amount. Toxicology. 2009;260(1–3):142–9. doi:10.1016/j.tox.2009.04.001.
58. Sterner T, Schutze N, Saxler G, Jakob F, Rader CP. Effects of clinically relevant alumina ceramic particles, circonia ceramic particles and titanium particles of different sizes and concentrations on TNF alpha release in a human monocytic cell line. Biomed Tech. 2004;49(12):340–4.
59. Fritz EA, Glant TT, Vermes C, Jacobs JJ, Roebuck KA. Chemokine gene activation in human bone marrow-derived osteoblasts following exposure to particulate wear debris. J Biomed Mater Res A. 2006;77A(1):192–201. doi:10.1002/jbm.a.30609.
60. Rodrigo A, Valles G, Saldana L, Rodriguez M, Martinez ME, Munuera L, et al. Alumina particles influence the interactions of cocultured osteoblasts and macrophages. J Orthop Res. 2006;24(1):46–54. doi:10.1002/jor.20007.
61. Renwick LC, Brown D, Clouter A, Donaldson K. Increased inflammation and altered macrophage chemotactic responses caused by two ultrafine particle types. Occup Environ Med. 2004;61(5):442–7. doi:10.1136/oem.2003.008227.
62. MacNee W, Donaldson K. Mechanism of lung injury caused by PM10 and ultrafine particles with special reference to COPD. Eur Resp J. 2003;21:475–515. doi:10.1183/09031936.03.00403203.
63. Valles G, Gonzalez-Melendi P, Gonzalez-Carrasco JL, Saldana L, Sanchez-Sabate E, Munuera L, et al. Differential inflammatory macrophage response to rutile and titanium particles. Biomaterials. 2006;27(30):5199–211. doi:10.1016/j.biomaterials.2006.05.045.
64. Palomaki J, Karisola P, Pylkkanen L, Savolainen K, Alenius H. Engineered nanomaterials cause cytotoxicity and activation on mouse antigen presenting cells. Toxicology. 2010;267(1–3):125–31. doi:10.1016/j.tox.2009.10.034.